RESEARCH ARTICLE

The shape effect of flagella is more important than bottom-heaviness on passive gravitactic orientation in *Chlamydomonas reinhardtii*

Azusa Kage*,‡,§, Toshihiro Omori‡, Kenji Kikuchi and Takuji Ishikawa

ABSTRACT

The way the unicellular, biflagellated, green alga *Chlamydomonas* orients upward has long been discussed in terms of both mechanics and physiology. In this study, we focus on the mechanics, i.e. the 'passive' mechanisms, of gravitaxis. To rotate the body upwards, cellular asymmetry is critical. *Chlamydomonas* can be depicted as a nearly spherical cell body with two anterior, symmetric flagella. The present study looks at the question of whether the existence of the flagella significantly affects torque generation in upward reorientation. The 'density asymmetry model' assumes that the cell is spherical and bottom-heavy and that the shape and weight of the flagella are negligible, while the 'shape asymmetry model' considers the shape of the flagella. Both our experimental and simulation results revealed a considerable contribution from shape asymmetry to the upward orientation of *Chlamydomonas reinhardtii*, which was several times larger than that of density asymmetry. From the experimental results, we also quantified the extent of bottom-heaviness, i.e. the distance between the centers of gravity and the figure when the cell body is assumed to be spherical. Our estimation was approximately 30 nm, only one-third of previous assumptions. These findings indicate the importance of the viscous drag of the flagella to the upward orientation, and thus negative gravitaxis, in *Chlamydomonas*.

KEY WORDS: Gravitaxis, Eukaryotic flagella, Cell asymmetry, Microalga, Microswimmer

INTRODUCTION

Taxis leads an organism to find optimal conditions in which to live. Negative gravitaxis, or migration against gravity, plays a role in the vertical migration of planktonic microorganisms, enabling them to acquire food and oxygen, and move into areas of optimal salinity or intensity of light (Chia et al., 1984; Erga et al., 2015). As a driving force of bioconvection (Wager, 1911; Kage et al., 2011, 2013; Kage and Mogami, 2015), it is also potentially important in the field of collective dynamics, such as red tide (Bearon and Grünbaum, 2008). Both mechanics and physiology are involved in the process of negative gravitactic behavior, the extent of which depends on the species of the organism. Here, we focus on the mechanics of

gravitaxis in the puller-type microalga *Chlamydomonas reinhardtii* Dangeard 1888, the model biflagellate for biophysical studies of cell motility.

Chlamydomonas is a unicellular organism with two anterior flagella, whose gravitaxis has been investigated from both experimental and theoretical perspectives (Bean, 1977; Vladimirov et al., 2004; Kessler, 1985; Roberts, 2006). Both physiology and mechanics are important in the mechanism of negative gravitaxis in *Chlamydomonas*. In mechanics, physical asymmetry is a key factor in exerting torques that reorient the body upward. The 'density asymmetry model' simplifies the description of the *Chlamydomonas* cell as a bottom-heavy sphere, and neglects the shape or weight of flagella. Flagella are modeled as a driving force without physical entity (Fig. 1B; Kessler, 1985). In contrast, the 'shape asymmetry model' considers the shape of flagella as the origin of asymmetry (Fig. 1C; Roberts, 1970, 1972, 2006). In this model, thin rods that represent flagella are connected to a sphere of identical density. If this 'cell' is heavier than the surrounding medium (i.e. the medium is hypodense), the sphere sinks faster than the rods and thus the 'cell' orients upwards as a whole. The actual cells are usually heavier than the medium, so that this mechanism can work in an actual situation.

The dominance of the two 'passive' models can be experimentally distinguished by the orientation of cells in a hyperdense medium, i.e. a medium heavier than the cells (Hosoya et al., 2010). The idea is that (1) if density asymmetry is dominant, then the cells will orient upward in a hyperdense medium because bottom-heaviness makes the posterior of the cell point downward regardless of the medium density; alternatively, (2) if shape asymmetry is dominant, then the cells will orient downward, because the sphere floats faster than the thin rods. Based on this idea, Hosoya et al. (2010) showed the emergence of 'reverse bioconvection' of *C. reinhardtii* in a hyperdense medium, i.e. accumulation at the bottom of the chamber initially. This result suggested that in *C. reinhardtii*, shape asymmetry is dominant over density asymmetry. Although it could be the basis for further investigation, the authors only showed population-level dynamics and did not present quantitative data on individual behavior.

The present study quantitatively investigated the dynamics of individual cells in negative gravitaxis of *C. reinhardtii*. To test the present hypothesis that shape asymmetry is the dominant mechanism for exerting the torque that rotates the body upward, we deflagellated or immobilized the *C. reinhardtii* cells and let them fall down. Based on flagellar waveform taken from experimental images, we further investigated upward rotation in a swimming cell. Our results indicated the substantial contribution of shape asymmetry, supporting the previous experimental results of Hosoya et al. (2010). Further, our data revealed a passive reorientation mechanism in the negative gravitaxis of *C. reinhardtii*.

Department of Finemechanics, School of Engineering, Tohoku University, 6-6-01 Aramaki Aza Aoba, Sendai, Miyagi 980-8579, Japan.
*Present address: Department of Mechanical Engineering, Toyohashi University of Technology, 1-1 Hibarigaoka, Tempaku, Toyohashi, Aichi 441-8580, Japan.
‡These authors contributed equally to this work

§Author for correspondence (kage@me.tut.ac.jp)

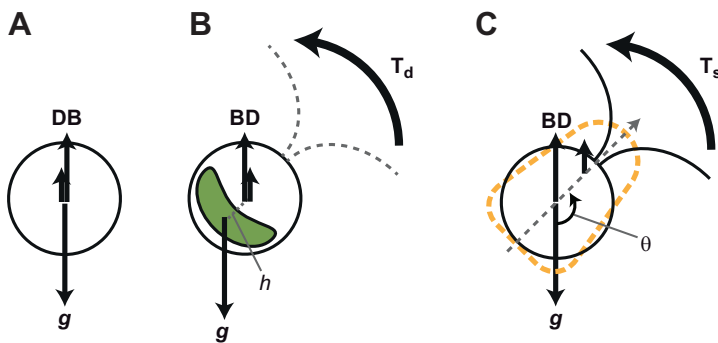A.K., 0000-0003-3069-3162; K.K., 0000-0001-8187-6773; T.I., 0000-0002-3573-8414

Fig. 1. Mechanics of passive upward orientation in *Chlamydomonas reinhardtii*. (A) No torque is generated without asymmetry because the centers of gravity, buoyancy and drag are all the same as the center of geometry. (B) The fore–aft density asymmetry model, neglecting the flagella to generate upward torque and considering *C. reinhardtii* as a 'bottom-heavy' sphere (Kessler, 1985). Upward torque is generated if the center of gravity is located posterior to the centers of buoyancy and drag. The center-of-gravity offset, *h*, the distance between the centers of gravity and geometry, indicates the extent of bottom-heaviness. (C) The fore–aft shape asymmetry model. When we considered the flagella, the shape-effect owing to the presence of flagella causes the center of drag to be located anterior to the centers of buoyancy and drag. *g*, gravity; **B**, buoyancy; **D**, drag; T_d, torque caused by density asymmetry; T_s, torque caused by shape asymmetry; θ, body orientation angle to gravity.

MATERIALS AND METHODS

Cell culture

Chlamydomonas reinhardtii strain 137c wild type, originally derived from the Kamiya Lab (formerly at the University of Tokyo), was used (Kage et al., 2013). Briefly, cells were cultivated in a sterile TAP medium with gentle aeration. Cells in mid-log phase were harvested for experiments.

Deflagellation and immobilization

To compare cells with and without flagella, part of each culture was deflagellated by means of pH shock. A volume of 30 µl of 1 mol l^{-1} acetic acid was added to a 1.0 ml cell suspension. After 45 s of mild mechanical agitation, it was neutralized with KOH solution. To analyze passive falling dynamics, suspensions were diluted with fresh TAP medium to a density of 1×10^5 cells ml^{-1} and cells were mildly fixed with glutaraldehyde (final concentration ∼0.1%). Before each experiment, we confirmed the presence or absence of flagella and checked for anomalies in cell shape using optical microscopy. The samples were then transferred into an experimental chamber made of a slide and cover glass, with a 0.5-mm silicone rubber sheet with a 10×10 mm square hole between them.

Analysis of vertical movement

To analyze the falling dynamics of the immobilized cells, we developed a horizontal fluorescent microscope system (Fig. 2). We placed a digital microscope (CX-10C; Hirox, Tokyo, Japan) horizontally and obtained time-series stacks of fluorescent images of *C. reinhardtii* falling down with rotation. A beam from a metal halide lamp (LA-180Me; Hayashi Watch-Works Co., Ltd, Tokyo, Japan) was irradiated from the back of the experimental chamber through a bandpass filter with wavelengths of 460–495 nm (BP460-495; Olympus, Tokyo, Japan). A fluorescent image was obtained with an absorption filter (<510 nm; BA510IF; Olympus), a dichroic mirror (DM505; Olympus) and an EMCCD camera (iXon+; Andor Technology Ltd, Belfast, Northern Ireland). A stack of images with a given frame rate could be obtained using this configuration, typically 31.2 frames s^{-1}. We rotated the experimental chamber upright and then upside down, having the cells inside fall down. The

image size was 512×512 pixels. To obtain the representative images shown in Fig. 3A, we used an inverted microscope and a high-resolution CCD camera (IX71 and DP73; Olympus) with the same filter set as described above (Fig. 3B).

Image analysis and rotational velocity

The orientation of the *C. reinhardtii* cells was determined by visual inspection, using the 'cup shape' of chloroplast autofluorescence, drawing a line vertical to the 'bottom' of the U-shape using Bohboh image processing software (Bohbohsoft, Tokyo, Japan). The angle θ of the line to gravity was used to calculate rotational velocity Ω. A time series of the angle θ to the gravitational direction was obtained for each cell. The rotational velocity was calculated from cells with angle θ to gravity of $1/3\pi$–$2/3\pi$ rad. The upward rotational velocity was expected to be maximal when the angle of the cell was horizontal to gravity (Roberts, 2006; Mogami et al., 2001). The rotational velocity, Ω, in Fig. 4 was obtained from the first and last frames in each stack of images of a cell. The statistical analysis was conducted using R (www.r-project.org) or Python. Rotational velocity was predicted from the shape of flagella and the orientation of the cell using the boundary element–slender body theory coupling method (see Appendix 2) with an aspect ratio of cell body 1.2 (prolate, minor radius 5 µm) and flagellar length 12 µm. The center-of-gravity offset, *h*, was set at 30 nm for computational analysis (see below). The other physical parameters are summarized in Table 1.

Center-of-gravity offset

The center-of-gravity offset, *h* (Fig. 1B), was obtained by fitting the integrated form of Eqn A3 (described in Appendix 1) to the time-series of the experimental data from the deflagellated cells using the least-squares method. Because we could obtain exact values for the major and minor axes of cells from the fluorescent images of a chloroplast, the parameters were assumed to be the same as the median values measured from the phase contrast images of the deflagellated cells in the same culture, which had been taken in advance of the horizontal fluorescent microscopy to confirm the absence of flagella. The values used for each culture were 4.6–5.0 and 5.2–6.2 µm for the minor and the major radii, respectively, and
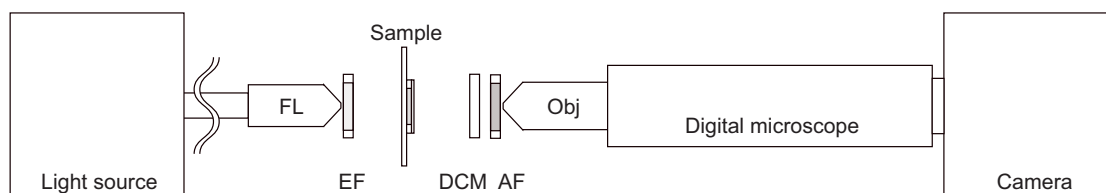

Fig. 2. Schematic side view of experimental setup. FL, focusing lens; EF, excitation filter; DCM, dichroic mirror; AF, absorption filter; Obj, objective lens. The sample chamber was made of a glass slide and coverslip, with a silicone rubber spacer between them.
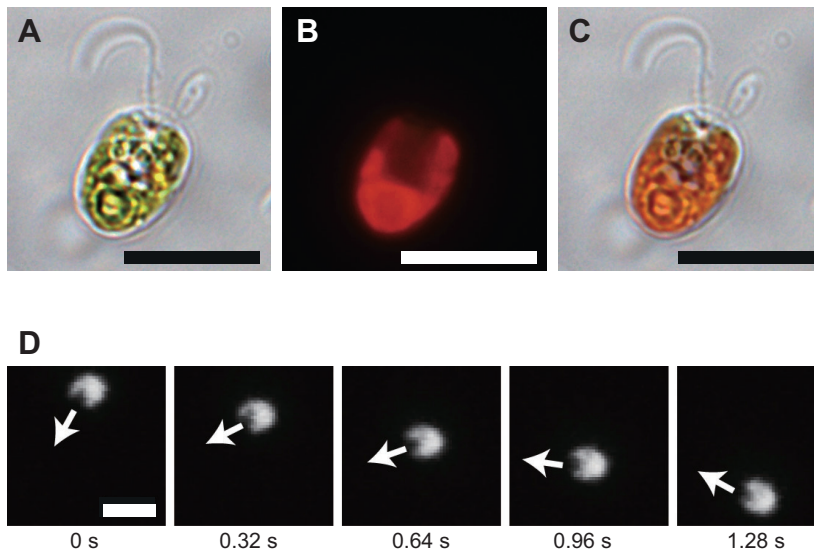
Fig. 3. Chloroplast autofluorescence of
Chlamydomonas reinhardtii. (A–C) A representative
image of autofluorescence. The 'cup shape' of the
chloroplast was used to distinguish the anterior
(flagellated) and posterior parts of the cell.
(A) Differential interference contrast image;
(B) fluorescent image; (C) merged image of A and B.
(D) Example of a flagellated cell falling down with
rotation. Arrows indicate the directions of the cell
determined by eye. Scale bars: 10 μm. The label
showing the direction
of gravity is to the right.

the aspect ratio was 1.14–1.27 with a prolate shape. The derivation of h is shown in Appendix 1.

Rotational velocity of a swimming cell
A sequence of flagellar waveforms was traced from images of a wild-type cell recorded at 2000 frames s^{-1} with an upright microscope (Olympus BX51WI, ×100 objective, Olympus UPLSAPO, NA=1.40) and a high-speed camera (Photoron SA3). The rotational velocities predicted from each waveform were computed by the boundary element–slender body theory coupling method (see Appendix 2).

Swimming trajectory of living cells
Trajectories of swimming cells were recorded using a laboratory-made horizontal microscope with a ×10 objective lens (Olympus SPlan 10NH) and a CMOS camera (iDS UI-3250CP-M-GL) at 15 frames s^{-1}. Cells in mid-log phase were harvested as described above, centrifuged at 300 g for 4 min, and resuspended in the experimental solution containing 1 mmol l^{-1} KCl, 0.3 mmol l^{-1} CaCl$_2$, 0.1 mmol l^{-1} EGTA and 1 mmol l^{-1} Hepes (pH=7.6; modified from Yoshimura et al., 2003 and Hosoya et al., 2010). Swimming behavior was recorded in a chamber of slide and cover glasses with an 80-μm spacer (double-sided tape W-12, 3M), blocked with 1% bovine serum albumin (A7030, Sigma-Aldrich) to prevent the cells from sticking to the glass. The chamber was kept vertical as in the falling experiment. To avoid phototaxis, the recording system was kept in a darkened room and the *C. reinhardtii* cells were illuminated with a red light with a sharp-cut filter (SC-64, Fujifilm, Tokyo, Japan; Kage and Mogami, 2015). The swimming cells were tracked with the TrackMate plugin in ImageJ (Tinevez et al., 2017). To analyze turning behavior, 14 trajectories ranging from 157 to 339 frames were selected from 1390 tracking results, with a filter of beginning angles (less than $\pi/8$ rad to gravity) and angles near the end point (more than $7\pi/8$ rad to gravity). We selected those trajectories to clarify turning behavior from down to up. All the tracks are included in Dataset 1.

RESULTS
Flagellation increased rotational velocity several-fold
To determine the effect of flagella on upward rotation, we compared immobilized cells with and without flagella. We deflagellated the

C. reinhardtii cells and compared their rotational velocity when falling down with the flagellated and fixed (dead) cells. A previous study (Yoshimura et al., 2003) used flagella themselves to indicate cell orientation under dark-field illumination. However, this method could not be applied to the deflagellated cells because of the absence of flagella. We solved this problem by using cup-shaped chloroplast autofluorescence (Fig. 3B), and successfully visualized the body orientation in a time sequence (Fig. 3D).

We attempted theoretical prediction of rotational velocity under the assumption that flagella were all straight and kept the same shape with an angle χ to each other (Fig. 4A). The results indicated that the rotational velocity was maximum at the body orientation $\theta=\pi/2$ and minimum at $\theta=0$ and π, as indicated from Fig. 4B. The opening angle of flagella χ changed the rotational velocity by approximately 3-fold, with a maximum of 0.302 rad s^{-1} at $\chi=0$. The cells without flagella rotated less than 0.03 rad s^{-1}.

The experimental results were in line with our prediction (Fig. 4C). Because rotational velocity is theoretically maximized when the angle of the body to gravity θ equals $\pi/2$, we analyzed the rotational velocity in cells within the range of $1/3\pi \lesssim \theta \lesssim 2/3\pi$ in a series of experiments. Flagellated and immobilized cells showed upward rotation with a ratio of 0.050–0.231 rad s^{-1} and a median of 0.118 rad s^{-1} (N=18), while the rotational velocity of deflagellated cells ranged from 0 to 0.228 rad s^{-1} with a median of 0.037 rad s^{-1} (N=13). As shown in Fig. 4C, the maximum value in the deflagellated group was so large an outlier and almost equal to the maximum in the flagellated group that we thought we had failed to properly deflagellate the cell. A comparison of the experiments showed the presence of flagella significantly increased the upward rotational velocity ($P<10^{-4}$; Mann–Whitney U-test). The values obtained were roughly consistent with our prediction, suggesting that our assumption was adequate. The results indicated a substantial viscous drag of flagella, i.e. a shape effect, on the passive upward torque generation in *C. reinhardtii*. The time series of rotations (Fig. 4D,E) showed fluctuations in the deflagellated cells (Fig. 4D), suggesting substantial noise in measurement, in contrast to the flagellated cells (Fig. 4E). The translational velocities of the falling cells were in the order of 10^{-6} m s^{-1} (1.42–7.27 μm s^{-1} with a median of 2.42 μm s^{-1}), consistent with our prediction from the Stokes equation (1.67×10^{-6} m s^{-1}).
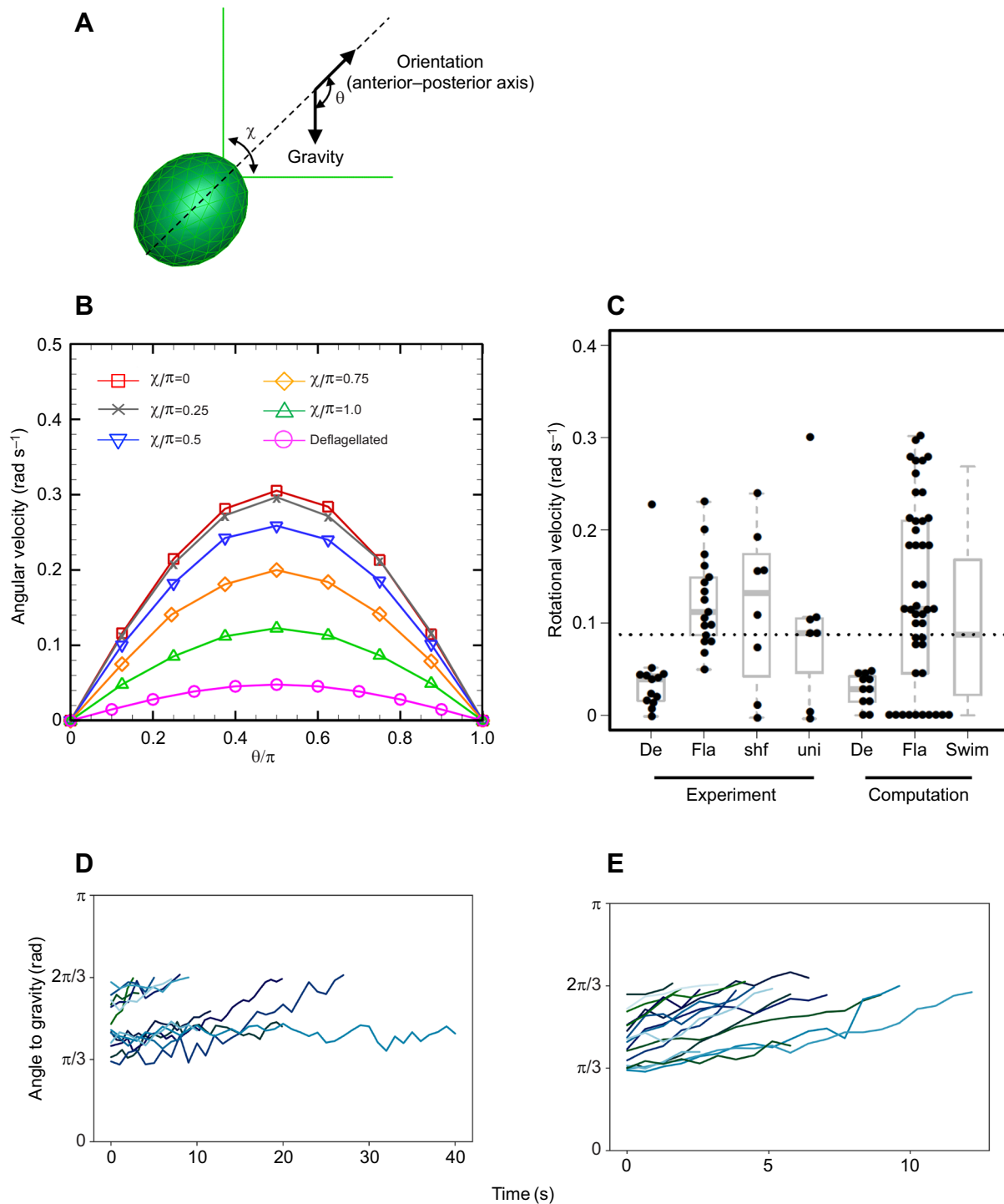
Fig. 4. Comparison of rotational velocity of the flagellated, immobilized and deflagellated cells. (A) Scheme of computation. χ, the angle between two flagella; θ, the angle of the body axis to gravity. (B) The angular velocities by computation with χ and θ changed. Each line indicates the results of different χ (χ/π=0.0, 0.25, 0.5, 0.75 and 1.0). The angular velocity is maximized when θ=π/2 and χ=0. (C) Comparison of experimental data (Experiment) to simulation results (Computation). Data points in computational results show the same points as in B. De, deflagellated wild type; Fla, flagellated wild type; shf, shf1-277 mutant; uni: uni1-1 mutant; Swim, simulation results with the flagella moving (see Fig. 6 and Appendix 2). The dotted line shows the value of flagellated cells from Yoshimura et al. (2003). (D) Time course of deflagellated cells. (E) Time course of flagellated cells.

Rotational velocities of immobilized, uniflagellated uni1-1 (a gift of Dr Masafumi Hirono, Hosei University, Japan) and short-flagellated shf1-277 (CC-2347, Chlamydomonas Resource Center) mutants ranged from −0.007 to 0.315 rad s^{-1} and from −0.006 to 0.235 rad s^{-1}, respectively (Fig. 4C). Both had a

broad distribution that covers the range of flagellated and deflagellated wild-type cells. The subtle rotation might have been because some portion of the cells lacked flagella in these mutants. In contrast, the length and number (one or two) of flagella did not have a significant effect on overall rotational velocity. The

Table 1. Physical parameters used in numerical simulations

Gravity, g	9.8 m s^{-2}
Viscosity, μ	1 mPa.s
Density difference, $\Delta\rho$	30 kg m^{-3}
Body radius, a	5 µm
Aspect ratio, a/b	1 to 1.3
Flagellar length, L	12 µm
Flagellar radius, a_{fla}	100 nm
Slenderness, $\varepsilon=a_{fla}/L$	8.3×10^{-3}
Beat frequency, f_{beat}	50 Hz
Offset, h	30 nm

rotational velocity was affected by the geometry of flagella rather than the aspect ratio of the cell body (Fig. S1).

Estimation of the center-of-gravity offset, h

Using the experimental rotational velocity data and the dimensions of the deflagellated cells, we calculated the center-of-gravity offset, h (Fig. 1B), i.e. the distance from the center of gravity to the center of geometry, which indicates the extent of 'bottom-heaviness'. The h of each cell was calculated from the time change in $\tan(\theta/2)$ by fitting Eqn A4, as shown in Fig. 5A. The result yielded a median of 28 nm (range: 14–54 nm; see Fig. 5B). The maximum, 54 nm, was an outlier ($N=10$). The median value was 27 nm and approximately 30% of the previous assumption of 100 nm used by Kessler (1986) and Jones et al. (1994). We used $h=30$ nm in the calculation described in this paper unless otherwise stated.
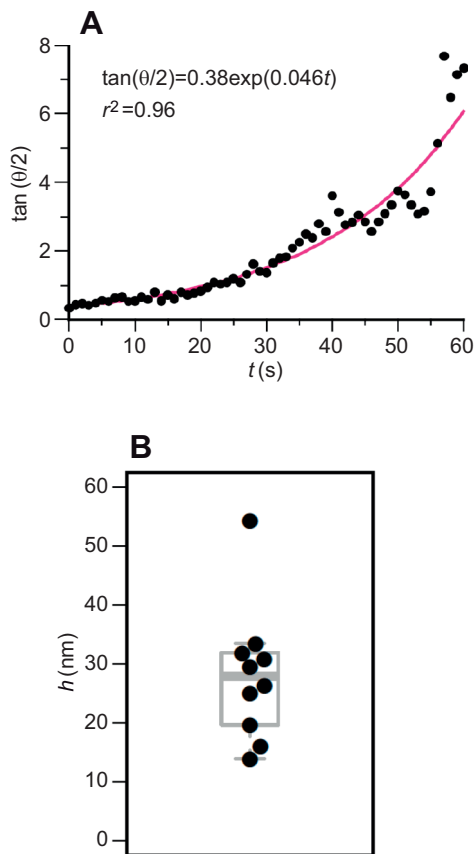

Fig. 5. Calculation of the center-of-gravity offset, h, from the experimental data. (A) Example of fitting to calculate h. (B) Boxplot for h. The median was 28 nm, the maximum was 54 nm (an outlier) and the minimum was 14 nm. $n=10$.

Swimming effect on rotational velocity in a motile cell

Our experiments showed that the presence of flagella increased upward rotational velocity in immotile cells. In order to evaluate the effect of flagellar beat in motile cells, we simulated a swimming cell based on experimental data (Fig. 6A). A planar waveform of *C. reinhardtii* was taken from an experimental recording. The time sequence of a flagellar waveform during one period is shown in the recording. Owing to the effective stroke ($2/5 \leq t/T \leq 7/8$, where T is the period), the cell could swim forwards, whereas it swam backwards in the recovery phase. Though the cell showed forward/backward swimming during the period, overall, the cell swam forwards, against the gravitational force. Rotational velocity was greatest at the end of recovery stroke and least at the beginning of recovery stroke. At $\pi/2 \leq \theta \leq \pi$, rotational velocity decreased with increasing θ, as expected from the governing equation. The time-averaged rotational velocity of the motile cell was 0.172 rad s^{-1} at $\theta=\pi/2$, 0.160 rad s^{-1} at $\theta=5\pi/8$, 0.123 rad s^{-1} at $\theta=3\pi/4$ and 0.0672 rad s^{-1} at $\theta=7\pi/8$. These values are comparable to both experimental and theoretical values in immotile, flagellated cells (Fig. 4C).

Living cells showed steep turning

Fig. 7 illustrates the swimming trajectory of living cells recorded in low magnification for more than 10 s. As seen in Fig. 7A, the cells turned direction and reoriented finally upwards. Fig. 7B shows the time course of y coordinates, showing an upward/downward movement of the cells. The plots are V-shaped (Fig. 7B, 3–14) rather than U-shaped (Fig. 7B, 1 and 2), indicating a steep reorientation in gravitational direction at the bottom of the trajectories. Fig. 7C shows the time course of the swimming angle ξ to gravitational direction, which shifts from near zero to near π over time. In order to roughly estimate the rotational velocity when swimming, we conducted linear regression with an assumption of $\xi=Ct$, where C (rad s^{-1}), the turning ratio, is a constant. The results yielded a C-value of 0.144–0.364 rad s^{-1} with a median of 0.213 rad s^{-1}, which agreed well with the experimental and computational results of immotile cells (Fig. 4C) and the simulation results of a swimming cell (Fig. 6). Although we fitted a linear function for simplicity, the angle did not always increase linearly or smoothly, as seen in most of the plots in Fig. 7C. These steep reorientations might reflect discontinuity in swimming behavior such as changing flagellar waveform or asynchrony between flagella.

DISCUSSION

By combining experimental and numerical approaches, we were able to show that the presence of flagella plays an important role in the passive upward torque generation of *C. reinhardtii*. This finding is in contrast to the common assumption that the shape effect of flagella can be neglected. We estimated the center-of-gravity offset, h, based on deflagellated cell experimental data and showed that h was approximately one-third of the previous theoretical assumptions (Jones et al., 1994; Kessler, 1986). We quantitatively estimated the density and shape effects of swimming cells using the boundary element method, showing that the shape effect is several times larger than the density effect, regardless of the initial body angles. These results illustrate that gravitactic behaviors can be altered by a flagellar waveform, which is likely to support the experimental results of Kage and Mogami (2015), that swimming direction is more upwardly biased in the *ida1* mutant of *C. reinhardtii*.

Our present results do not exclude the active physiological reorientation mechanism in negative gravitaxis of *Chlamydomonas* depicted by Bean (1977) or Yoshimura et al. (2003).
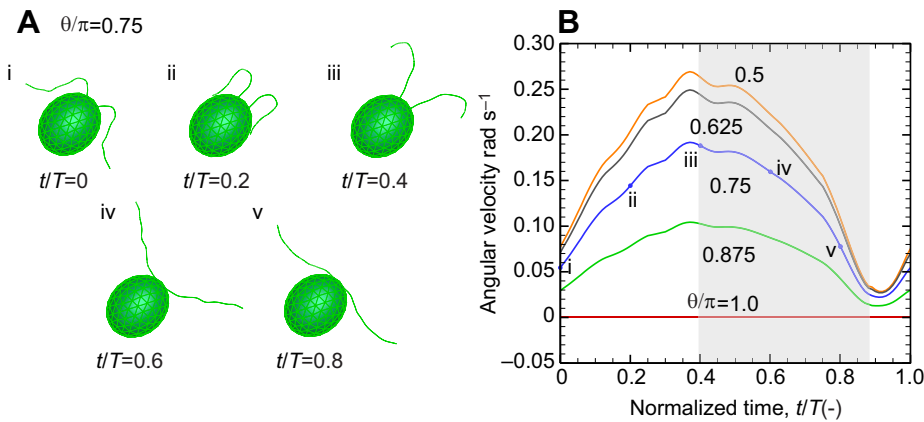
Fig. 6. Rotational velocity of swimming cell during one period of flagellar beat. (A) The flagellar waveform was traced from the sequence of experimental data. The aspect ratio of the cell body was fixed as 1.2 (prolate). i–v correspond to the times indicated in B. (B) Rotational velocity was calculated from the flagellar waveform shown in A. Shaded region indicates effective stroke.

Bean (1977) described three types of reorientation mechanisms: (i) physical interaction of the cell with another object; (ii) spontaneous angular turn in swimming direction; and (iii) smooth gradual continuous low-angle turn, which would be in the scope of our present results. Mechanisms i and ii could be interpreted as waveform changes, such as a photophobic response (Kröger and Hegemann, 1994), or flagellar asynchrony (Polin et al., 2009) owing to mechanical shock or spontaneous changes in membrane potential, whereas mechanism iii could be interpreted as a natural rotation in the swimming direction. As shown in Fig. 6B, swimming cells rotate upwards with a time-averaged angular velocity of 0.172 rad s^{-1} to nearly 0 rad s^{-1}, depending on body orientation θ. This should also be the case for slowly reorienting cells. Bean (1977), for instance, reported '20–50 deg angle changes in the swimming vector of the cell during the 3.3 s period' for mechanism iii. If a cell obeys this rotation rate (Fig. 8), it would take it approximately 47 s to reorient from the angle near 0 (downwards) to near π (upwards), as indicated from the boundary element method simulation results from 0.01π to 0.99π. In contrast, our observation of vertical swimming showed a reorientation time of approximately 10–22 s, although the reorientation rate was not uniform and rapid reorientation in a few seconds often occurred (Fig. 7). Steep turning, as shown in Fig. 7, implies changes in waveform or asynchrony between flagella. Active processes might alter the relative synchrony between flagella or in the flagellar waveform itself, thereby leading to an additional reorientation torque. Yoshimura et al. (2003) isolated mutants that did not show negative gravitaxis, although their physical characteristics including swimming velocity, and flagellar beat frequency were similar to those of the wild type. Mutants with defects in their photophobic response might have defects in rapid turning in gravitaxis as well.

Although the present experiment deals only with a few strains of *C. reinhardtii*, our results can be generalized when exploring the mechanism of gravitaxis in a biflagellate. In addition, *C. reinhardtii* has an advantage among biflagellates, or pullers, because it is a model organism for biology (Harris, 2009), and information on its genetics and physiology is extensively available compared with other species of biflagellates. Some British groups have used *Chlamydomonas nivalis* (Kessler, 1985) or *Chlamydomonas augustae* (CCAP11/51B, Williams and Bees, 2011; which is identical to SAG26.86 or UTEX1969). These strains have been reclassified as *Chloromonas typhlos* (Matsuzaki et al., 2012), and are now not even included in the genus *Chlamydomonas*. However, their physical entity and their similarity with *Chlamydomonas* remains unchanged, although we still emphasize the advantage of *C. reinhardtii* as a model organism that has a number of mutants

available with genetic methods established, while the physiology and genetics of *C. nivalis* used by Kessler (1985) are not well understood and need further investigation. Clarifying the swimming properties of *C. reinhardtii* could be more useful for future studies, particularly when we consider the hierarchical properties of bioconvection or collective motion.

O'Malley and Bees (2012) were also aware of the possibility that the shape effect of flagella might be important for the upward reorientation of biflagellated microorganisms such as *Chlamydomonas*. They numerically explored the shape effect of flagella, among which were complex waveforms mimicking *C. reinhardtii* based on the waveform taken experimentally by Ringo (1967) and Rüffer and Nultsch (1985). The conclusion by O'Malley and Bees (2012) was that both 'bottom-heaviness' and 'sedimentation' mechanisms are 'equally important' (O'Malley and Bees, 2012). From their estimate of the maximum orientation rate β, i.e. angular velocity, Ω_s/Ω_d was in the range of 0.5–0.9, where Ω_s and Ω_d are the angular velocities generated by flagellar viscous drag and bottom-heaviness, respectively, if we use our expression (see table 1 in O'Malley and Bees, 2012). Based on our experimentally obtained value of *h*, we calculated $\Omega_s/\Omega_d \approx 6$ in a swimming cell. This value is much greater than the value O'Malley and Bees (2012) computed. The results of our experiment showed that the flagellar shape effect is much more important in upward reorientation of *Chlamydomonas* than previously considered.

As stated above, individual flagellar waveform has a substantial effect on collective behavior (Kage and Mogami, 2015). From our present data, flagellar conformation has a substantial effect on at least torque generation upwards. We suggest that it might be possible for the 'average flagellar waveform' in a population to drastically change collective behavior, even if we neglect physiological responses to mechanical stimuli, depending on strains. To date, many people have used the bottom-heaviness model in analyzing the motion of suspensions of cells (Goldstein, 2015; Hill and Pedley, 2005). Fortunately, the formula for the rate of reorientation of a cell differs only in a multiplicative constant, with the orientation-dependent factor sinθ the same for both models.

The present results suggest that the roles of cilia/flagella in gravitaxis may differ between a flagellate and a ciliate, given that flagellar drag could be negligible in ciliates. In a flagellate with few flagella, the drag derived from the shape of the flagella should have a substantial effect on its reorientation as in *Chlamydomonas*. This should not be the case in a ciliate that has many flagella (cilia) on its body and propels itself via the coordination of its cilia; even if the shape asymmetry worked in the reorientation mechanism in a ciliate such as *Paramecium*, that could not be attributed to the shape of the flagella. Rather, the asymmetry in the cell body would work.
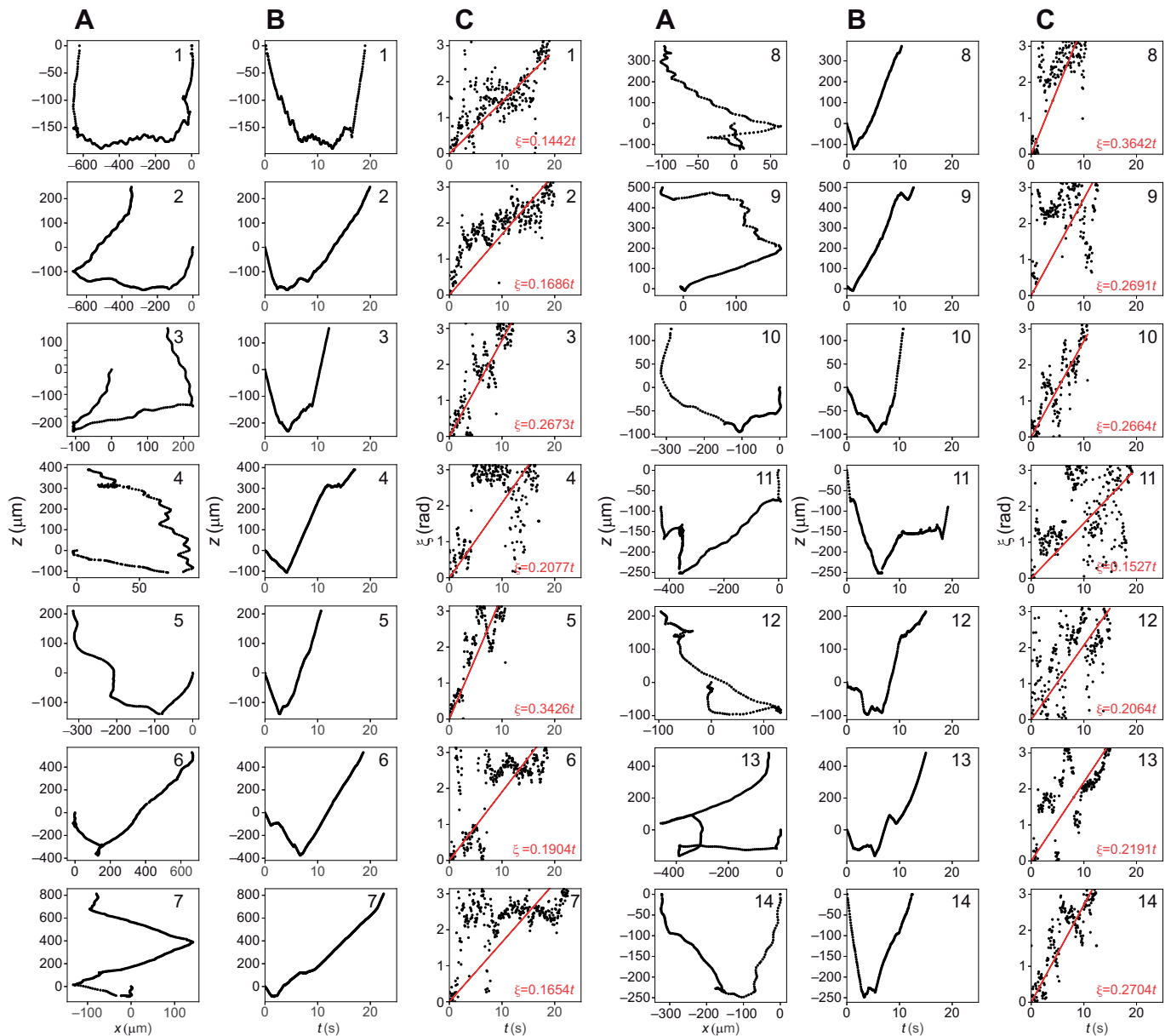
Fig. 7. Fourteen swimming trajectories of *C. reinhardtii*, showing it turning from downwards to upwards. Rows 1–14 correspond to each trajectory. (A) 2-D trajectories; (B) time course of *y* coordinates; (C) time course of the swimming angle ξ. Red lines indicate linear regression with intercept 0.

To conclude, the viscous drag of flagella plays an important role in the passive gravitaxis mechanism of *Chlamydomonas*. This result is important for understanding not only the mechanism of gravitaxis itself but also the collective dynamics of microorganisms driven by negative gravitaxis. Further studies should include the effects of both waveform and the trajectories of swimming cells on physiological regulation and signal transduction to establish a picture of gravitaxis in *Chlamydomonas* as a model swimming microorganism.

APPENDIX 1
Center-of-gravity offset, *h*

The density asymmetry torque, T_d, on a prolate ellipsoid is given by:

$$T_d = F_f h \sin\theta, \tag{A1}$$

where F_f is the gravity force. The viscous drag torque, T_v, of a prolate ellipsoid is expressed as:

$$T_v = \mu L_{11}\Omega(t), \tag{A2}$$

where μ is the viscosity of the surrounding water, L_{11} is the drag coefficient for a prolate ellipsoid and $\Omega(t)$ is the rotational velocity of the ellipsoid. Assuming a balance between the two torques, *h* can be derived as:

$$h = \frac{\mu L_{11}\Omega(t)}{F_f \sin\theta}. \tag{A3}$$

When the time series for $\Omega(t)$ was obtained directly from the measured values, there was substantial noise. To avoid this, we fitted the integrated form:

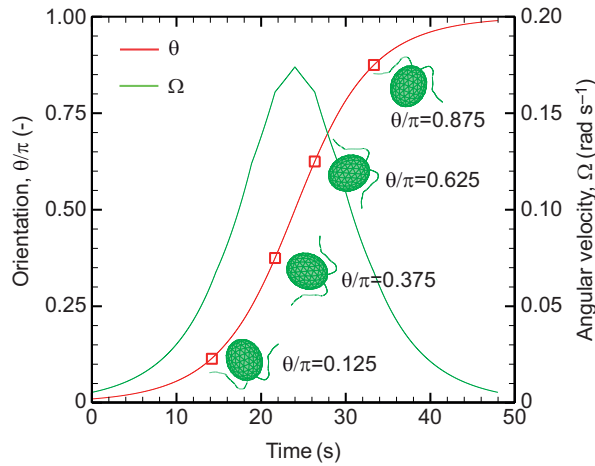$$\tan\frac{\theta(t)}{2} = c_2 \exp(c_1 t), \tag{A4}$$

Fig. 8. Numerical results of reorientation of the cell turning from downwards to upwards; orientation angle (red) and angular velocity (green). The cell was initially oriented to $\theta/\pi=0.01$.

to the measured values of θ (Fig. 5A), where $c_1=\dfrac{hF_f}{\mu L_{11}}$ and $c_2=\tan\dfrac{\theta(0)}{2}$.

APPENDIX 2
Numerical method
In this appendix, we explain the methodology of our numerical model. Assume that a model of *Chlamydomonas* is freely suspended in an incompressible Newtonian liquid with viscosity μ and density ρ_0. Also assume the cytoplasm has the viscosity μ but the density ρ. Owing to the small size of *Chlamydomonas*, the inertia effect of fluid motions can be set aside. The flow field is governed by the Stokes equation. The flow field can be then expressed by a boundary integral equation, which is solved by a boundary element method (Omori et al., 2012). We use a slender body theory (Tornberg and Shelley, 2004) for flagellar motions because its radius a_{fla} is sufficiently small compared with its length L ($a_{fla}/L\ll1$). The cell body is modeled as a prolate spheroid, the velocity field for points $\mathbf{x}$ outside, or on the cell surface is then given by:

$$\mathbf{v}(\mathbf{x})=-\frac{1}{8\pi\mu}\int\mathbf{J}(\mathbf{x},\mathbf{y})\cdot\mathbf{q}(\mathbf{y})\mathrm{d}S_{body}(\mathbf{y})+\mathrm{SBT}(\mathbf{x}),\qquad(A5)$$

where $\mathbf{q}$ is the viscous stress jump across the membrane, S indicates the cell body surface and $\mathbf{J}$ is the Green's function:

$$\mathbf{J}=\frac{\mathbf{I}}{r}+\frac{\mathbf{r}\otimes\mathbf{r}}{r^3},\qquad(A6)$$

where $\mathbf{I}$ is the identity matrix, $r=|\mathbf{r}|$, and $\mathbf{r}=\mathbf{y}-\mathbf{x}$. The last term in Eqn A5 represents the slender body term (SBT), which is given by (Tornberg and Shelley, 2004):

$$\mathrm{SBT}(\mathbf{x})=\begin{cases}-\dfrac{1}{8\pi\mu}\mathbf{\Lambda}(\mathbf{x})\cdot\mathbf{f}(\mathbf{x})-\dfrac{1}{8\pi\mu}\int[\mathbf{J}(\mathbf{x},\mathbf{y})\cdot\mathbf{f}(\mathbf{y})\\ \quad-\mathbf{K}(\mathbf{x},\mathbf{y})\cdot\mathbf{f}(\mathbf{x})]\mathrm{d}l_{fla}(\mathbf{y})\quad\text{if }\mathbf{x}\in\text{ flagella}\\ -\dfrac{1}{8\pi\mu}\int[\mathbf{J}(\mathbf{x},\mathbf{y})+\mathbf{W}(\mathbf{x},\mathbf{y})]\cdot\mathbf{f}(\mathbf{y})\mathrm{d}l_{fla}(\mathbf{y})\quad\text{otherwise,}\end{cases}$$
$$(A7)$$

where $\mathbf{f}$ is the viscous force per unit length acting on the flagella, $\mathbf{\Lambda}$ is the local operator:

$$\mathbf{\Lambda}(\mathbf{x})=c(\mathbf{I}+\mathbf{t}(\mathbf{x})\otimes\mathbf{t}(\mathbf{x}))+2(\mathbf{I}-\mathbf{t}(\mathbf{x})\otimes\mathbf{t}(\mathbf{x})),\qquad(A8)$$

$c=-\ln(\varepsilon^2 e)$, $\varepsilon=a_{fla}/L$ is the slenderness of the flagellum, $\mathbf{t}$ is the unit tangential vector, $\mathbf{K}$ is the integral operator:

$$\mathbf{K}(\mathbf{x},\mathbf{y})=\frac{\mathbf{I}+\mathbf{t}(\mathbf{x})\otimes\mathbf{t}(\mathbf{x})}{|s(\mathbf{x})-s(\mathbf{y})|},\qquad(A9)$$

$s\in[0, L]$ is the arclength of the flagellum, and $\mathbf{W}$ is:

$$\mathbf{W}=\frac{(\varepsilon L)^2}{2}\left[\frac{\mathbf{I}}{r^3}-3\frac{\mathbf{r}\otimes\mathbf{r}}{r^3}\right].\qquad(A10)$$

In order to simulate the free-swimming of *Chlamydomonas*, we need to consider the force and torque conditions of the cell. Because the cytoplasm is heavier than water, gravitational external force is taken into account, and we have the following force condition:

$$\int\mathbf{q}\mathrm{d}S_{body}+\int\mathbf{f}\mathrm{d}l_{fla}+\frac{4}{3}\pi ab^2\Delta\rho\mathbf{g}=0,\qquad(A11)$$

where $\mathbf{g}=(0, 0, -g)$ is the gravity force, and $\Delta\rho=\rho-\rho_0$ is the density difference of the cytoplasm and outer liquid. The torque condition is also given by:

$$\int\mathbf{q}\wedge(\mathbf{x}-\mathbf{x}_c)\mathrm{d}S_{body}+\int\mathbf{f}\wedge(\mathbf{x}-\mathbf{x}_c)\mathrm{d}l_{fla}+\frac{4}{3}\pi ab^2\rho h\mathbf{e}\wedge\mathbf{g}=0,\quad(A12)$$

where $\mathbf{x}_c$ is the geometric center of the cell body, $\mathbf{e}$ is the orientation vector and h is the offset between the geometric center and the gravitational center. The last term on the left-hand side of Eqn A12 expresses the bottom-heaviness of the cell, which is taken into account only when we employ the density asymmetry model.

To express the time-dependent flagellar beat, waveforms are taken from experimental recordings. From a 2D image of Movie 1, material points of the centerline of the flagellum are manually tracked and interpolated with respect to time and space using a cubic spline. Once the waveform during one period is given, we can calculate flagellar velocity with respect to the body frame v_{fla}. Consider the no-slip boundary condition, the velocity at the cell material point can be decomposed as:

$$\mathbf{v}(\mathbf{x})=\mathbf{V}+\mathbf{\Omega}\wedge(\mathbf{x}-\mathbf{x}_c)+\mathbf{v}_{fla}(\mathbf{x}),\qquad(A13)$$

where $\mathbf{V}$ and $\mathbf{\Omega}$ are the translational and angular velocity of the cell, respectively. Note that $v_{fla}=0$ when $\mathbf{x}$ is located on the cell body. We then solve the following resistance problem with respect to unknown variables $\mathbf{q}$, $\mathbf{f}$, $\mathbf{V}$ and $\mathbf{\Omega}$ using a lower and upper factorization technique:

$$\begin{bmatrix}\mathbf{J}&\mathbf{A}\\\mathbf{B}&0\end{bmatrix}\begin{bmatrix}\mathbf{q}\\\mathbf{f}\\\mathbf{V}\\\mathbf{\Omega}\end{bmatrix}=\begin{bmatrix}\mathbf{v}_{fla}\\0\\0\end{bmatrix}.\qquad(A14)$$

For more details about the numerical method, please refer to our former study (Omori and Ishikawa, 2016).

APPENDIX 3
Time-integration of angular velocity
To numerically track the orientation of *Chlamydomonas* from downwards to upwards, the angular velocity was integrated with respect to time. Because the angular velocity Ω was varied with the current orientation θ, we first computed Ω for each θ using the

boundary element method, as shown in Fig. 8 (green line). Once Ω was given, the orientation angle was given by $\theta(t)=\int_0^t \Omega(\theta)\mathrm{d}t$. The initial condition was set as $\theta(0)=0.01\pi$.

Supplementary information
Supplementary information available online at
http://jeb.biologists.org/lookup/doi/10.1242/jeb.205989.supplemental

References
Bean, B. (1977). Geotactic behavior of *Chlamydomonas*. *J. Protozool.* **24**, 394-401. doi:10.1111/j.1550-7408.1977.tb04759.x

Bearon, R. N. and Grünbaum, D. (2008). From individual behaviour to population models: a case study using swimming algae. *J. Theor. Biol.* **251**, 679-697. doi:10.1016/j.jtbi.2008.01.007

Brokaw, C. J. and Kamiya, R. (1987). Bending patterns of *Chlamydomonas* flagella: IV. Mutants with defects in inner and outer dynein arms indicate differences in dynein arm function. *Cell Motil. Cytoskeleton* **8**, 68-75. doi:10.1002/cm.970080110

Chia, F.-S., Buckland-Nicks, J. and Young, C. M. (1984). Locomotion of marine invertebrate larvae: a review. *Can. J. Zool.* **62**, 1205-1222. doi:10.1139/z84-176

Erga, S. R., Olseng, C. D. and Aarø, L. H. (2015). Growth and diel vertical migration patterns of the toxic dinoflagellate *Protoceratium reticulatum* in a water column with salinity stratification: the role of bioconvection and light. *Mar. Ecol. Prog. Ser.* **539**, 47-64. doi:10.3354/meps11488

Goldstein, R. E. (2015). Green algae as model organisms for biological fluid dynamics. *Annu. Rev. Fluid Mech.* **47**, 343-375. doi:10.1146/annurev-fluid-010313-141426

Harris, E. H. (2009). *The Chlamydomonas Sourcebook, Second Edition, Vol. 1: Introduction to Chlamydomonas and Its Laboratory Use*. Academic Press.

Hill, N. A. and Pedley, T. J. (2005). Bioconvection. *Fluid Dyn. Res.* **37**, 1-20. doi:10.1016/j.fluiddyn.2005.03.002

Hosoya, C., Akiyama, A., Kage, A., Baba, S. A. and Mogami, Y. (2010). Reverse bioconvection of *Chlamydomonas* in the hyper-density medium. *Biol. Sci. Space* **24**, 145-152. doi:10.2187/bss.24.145

Jones, M. S., Le Baron, L. and Pedley, T. J. (1994). Biflagellate gyrotaxis in a shear flow. *J. Fluid Mech.* **281**, 137-158. doi:10.1017/s002211209400306x

Kage, A. and Mogami, Y. (2015). Individual flagellar waveform affects collective behavior of *Chlamydomonas reinhardtii*. *Zool. Sci.* **32**, 396-404. doi:10.2108/zs150015

Kage, A., Asato, E., Chiba, Y., Wada, Y., Katsu-Kimura, Y., Kubota, A., Sawai, S., Niihori, M., Baba, S. A. and Mogami, Y. (2011). Gravity-dependent changes in bioconvection of *Tetrahymena* and *Chlamydomonas* during parabolic flight: increases in wave number induced by pre- and post-parabola hypergravity. *Zool. Sci.* **28**, 206-214. doi:10.2108/zsj.28.206

Kage, A., Hosoya, C., Baba, S. A. and Mogami, Y. (2013). Drastic reorganization of the bioconvection pattern of *Chlamydomonas*: quantitative analysis of the pattern transition response. *J. Exp. Biol.* **216**, 4557-4566. doi:10.1242/jeb.092791

Kessler, J. O. (1985). Hydrodynamic focusing of motile algal cells. *Nature* **313**, 218-220. doi:10.1038/313218a0

Kessler, J. O. (1986). Individual and collective fluid dynamics of swimming cells. *J. Fluid Mech.* **173**, 191-205. doi:10.1017/S0022112086001131

Kröger, P. and Hegemann, P. (1994). Photophobic responses and phototaxis in *Chlamydomonas* are triggered by a single rhodopsin photoreceptor. *FEBS Lett.* **341**, 5-9. doi:10.1016/0014-5793(94)80229-7

Matsuzaki, R., Hara, Y. and Nozaki, H. (2012). A taxonomic revision of *Chloromonas reticulata* (Volvocales, Chlorophyceae), the type species of the genus *Chloromonas*, based on multigene phylogeny and comparative light and electron microscopy. *Phycologia* **51**, 74-85. doi:10.2216/11-18.1

Mogami, Y., Ishii, J. and Baba, S. A. (2001). Theoretical and experimental dissection of gravity-dependent mechanical orientation in gravitactic microorganisms. *Biol. Bull.* **201**, 26-33. doi:10.2307/1543522

O'Malley, S. and Bees, M. A. (2012). The orientation of swimming biflagellates in shear flow. *Bull. Math. Biol.* **74**, 232-255. doi:10.1007/s11538-011-9673-1

Omori, T. and Ishikawa, T. (2016). Upward swimming of a sperm cell in shear flow. *Phys. Rev. E* **93**, 032402. doi:10.1103/PhysRevE.93.032402

Omori, T., Imai, Y., Yamaguchi, T. and Ishikawa, T. (2012). Reorientation of a non-spherical capsule in creeping shear flow. *Phys. Rev. Lett.* **108**, 138102. doi:10.1103/PhysRevLett.108.138102

Polin, M., Tuval, I., Drescher, K., Gollub, J. P. and Goldstein, R. E. (2009). *Chlamydomonas* swims with two 'gears' in a eukaryotic version of run-and-tumble locomotion. *Science* **325**, 487-490. doi:10.1126/science.1172667

Ringo, D. L. (1967). Flagellar motion and fine structure of the flagellar apparatus in *Chlamydomonas*. *J. Cell Biol.*, **33**, 543-571. doi:10.1083/jcb.33.3.543

Roberts, A. M. (1970). Geotaxis in motile micro-organisms. *J. Exp. Biol.* **53**, 687-699.

Roberts, A. M. (1972). Gravitational separation of X and Y spermatozoa. *Nature,* **238**, 223-225. doi:10.1038/238223a0

Roberts, A. M. (2006). Mechanisms of gravitaxis in *Chlamydomonas*. *Biol. Bull.* **210**, 78-80. doi:10.2307/4134597

Rüffer, U. and Nultsch, W. (1985). High-speed cinematographic analysis of the movement of *Chlamydomonas*. *Cell Motil. Cytoskelet.* **5**, 251-263. doi:10.1002/cm.970050307

Tinevez, J.-Y., Perry, N., Schindelin, J., Hoopes, G. M., Reynolds, G. D., Laplantine, E., Bednarek, S. Y., Shorte, S. L. and Eliceiri, K. W. (2017). TrackMate: an open and extensible platform for single-particle tracking. *Methods* **115**, 80-90. doi:10.1016/j.ymeth.2016.09.016

Tornberg, A.-K. and Shelley, M. J. (2004). Simulating the dynamics and interactions of flexible fibers in Stokes flows. *J. Comput. Phys.* **196**, 8-40. doi:10.1016/j.jcp.2003.10.017

Vladimirov, V. A., Wu, M. S. C., Pedley, T. J., Denissenko, P. V. and Zakhidova, S. G. (2004). Measurement of cell velocity distributions in populations of motile algae. *J. Exp. Biol.* **207**, 1203-1216. doi:10.1242/jeb.00881

Wager, H. (1911). The effect of gravity upon the movements and aggregation of *Euglena viridis*, Ehrb., and other micro-organisms. *Philos. Trans. R. Soc. Lond. B* **201**, 333-390. doi:10.1098/rstb.1911.0007

Williams, C. R. and Bees, M. A. (2011). A tale of three taxes: photo-gyro-gravitactic bioconvection. *J. Exp. Biol.* **214**, 2398-2408. doi:10.1242/jeb.051094

Yoshimura, K., Matsuo, Y. and Kamiya, R. (2003). Gravitaxis in *Chlamydomonas reinhardtii* studied with novel mutants. *Plant Cell Physiol.* **44**, 1112-1118. doi:10.1093/pcp/pcg134